J|A|C|S ARTICLES

Published on Web 05/27/2010

Multifunctional Mesoporous Composite Microspheres with Well-Designed Nanostructure: A Highly Integrated Catalyst System

Yonghui Deng, Yue Cai, Zhenkun Sun, Jia Liu, Chong Liu, Jing Wei, Wei Li, Chang Liu, Yao Wang, and Dongyuan Zhao*

Department of Chemistry, Shanghai Key Laboratory of Molecular Catalysis and Innovative Materials, and Advanced Materials Laboratory, Fudan University, Shanghai 200433, People's Republic of China

Received March 29, 2010; E-mail: dyzhao@fudan.edu.cn

Abstract: The precise control of the size, morphology, surface chemistry, and assembly process of each component is important to construction of integrated functional nanocomposites. We report here the fabrication of multifunctional microspheres which possess a core of nonporous silica-protected magnetite particles, transition layer of active gold nanoparticles, and an outer shell of ordered mesoporous silica with perpendicularly aligned pore channels. The well-designed microspheres have high magnetization (18.6 emu/g), large surface area (236 m^2/g), highly open mesopores (~2.2 nm), and stably confined but accessible Au nanoparticles and, as a result, show high performance in catalytic reduction of 4-nitrophenol (with conversion of 95% in 12 min), styrene epoxidation with high conversion (72%) and selectivity (80%), especial convenient magnetic separability, long life and good reusability. The unique nanostructure makes the microsphere to be a novel stable and approachable catalyst system for various catalytic industry processes.

1. Introduction

The rapid progress of nanoscience and nanotechnology has enabled researchers to material engineers on the molecular- and nanoscale to a great extent.[1] A large number of novel nanomaterials and nanostructures that exhibit fantastic physical, chemical, and biological properties have been created and demonstrated high potentials for biomedicine, catalysis, sensor, energy conversion, and so on.[2−6] Composite nanomaterials with well-defined structures have been extensively explored to realize the combination of respective properties of each component or achieve cooperatively enhanced performances.[7−14] Core−shell structured nanocomposites have become a rapidly growing research field in material community. In general, the core−shell nanostructures can be easily obtained through two pathways. One is the self-assembly of surfactants with different compositions or the supramolecular assembly based on molecular recognition,[10] and another is surface reaction or precipitation (deposition) on a preformed nanoobject through electrostatic assembly, covalently grafting, or affinity coating.[11−14] As an important family of advanced nanomaterials, magnetic microspheres with magnetically responsive core and functional shell have gained much attention due to their unique separable feature which makes it possible to realize selective capture of interest target objects from the complex samples,[15] magnetically controllable on−off reactions[16] and convenient recycling of magnetic carriers. So far, to improve their performance in practical applications, much work has been done to enhance magnetic responsiveness and surface areas, and addition of new functionalities by combining with other functional nanomaterials. A variety of microspheres with inorganic magnetic particles embedded in different matrixes have been reported for applications in information storage, bioseparation, bioimaging, enzyme immobilization, and catalysis.[12−23]

(1) Rao, C. N. R., Müller, A., Cheetham, A. K. *Nanomaterials Chemistry: Recent Developments and New Directions*; Wiley-VCH: Weinheim, 2007).
(2) Alivisatos, A. P. *Science* **1996**, *271*, 933–937.
(3) Huang, M. H.; Mao, S.; Feick, H.; Yan, H. Q.; Wu, Y. Y.; Kind, H.; Weber, E.; Russo, R.; Yang, P. D. *Science* **2001**, *292*, 1897–1899.
(4) Deng, Y. H.; Wang, C. C.; Shen, X. Z.; Yang, W. L.; Jin, L.; Gao, H.; Fu, S. K. *Chem.−Eur. J.* **2005**, *11*, 6006–6013.
(5) Wang, Z. L.; Song, J. H. *Science* **2006**, *312*, 242–246.
(6) Holland, B. T.; Blanford, C. F.; Stein, A. *Science* **1998**, *24*, 538–540.
(7) Mann, S. *Nat. Mater.* **2009**, *8*, 781–792.
(8) Warren, S. C.; Disalvo, F. J.; Wiesner, U. *Nat. Mater.* **2007**, *6*, 156–161.
(9) Deng, Y. H.; Deng, C. H.; Yang, D.; Wang, C. C.; Fu, S. K.; Zhang, X. M. *Chem. Commun.* **2005**, 5548–5550.
(10) Jenekhe, S. A.; Chen, X. L. *Science* **1998**, *279*, 1903–1907.
(11) Caruso, F.; Caruso, R. A.; Möhwald, H. *Science* **1998**, *282*, 1111–1114.
(12) Liz-Marzán, L. M.; Giersig, M.; Mulvaney, P. *Langmuir* **1996**, *12*, 4329–4335.
(13) Xu, Z. H.; Hou, Y. L.; Sun, S. H. *J. Am. Chem. Soc.* **2007**, *129*, 8698–8699.
(14) Deng, Y. H.; Yang, W. L.; Wang, C. C.; Fu, S. K. *Adv. Mater.* **2003**, *15*, 1729–1732.
(15) Gupta, A. K. *Biomaterials* **2005**, *26*, 3995–4021.
(16) Katz, E.; Willner, I. *Angew. Chem., Int. Ed.* **2004**, *43*, 6042–6108.
(17) Park, J.; An, K. J.; Hwang, Y. S.; Park, J. G.; Noh, H. J.; Kim, J. Y.; Park, J. H.; Hwang, N. M.; Hyeon, T. *Nat. Mater.* **2004**, *3*, 891–895.
(18) Lu, A. H.; Salabas, E. L.; Schuth, F. *Angew. Chem., Int. Ed.* **2007**, *46*, 1222–1244.
(19) Deng, Y. H.; Qi, D. W.; Deng, C. H.; Zhang, X. M.; Zhao, D. Y. *J. Am. Chem. Soc.* **2008**, *130*, 28–29.
(20) Ge, J. P.; Zhang, Q.; Zhang, T. R.; Yin, Y. D. *Angew. Chem., Int. Ed.* **2008**, *47*, 8924–8928.
(21) Zhang, L.; Qiao, S. Z.; Jin, Y. G.; Chen, Z. G.; Gu, H. C.; Lu, G. Q. *Adv. Mater.* **2008**, *20*, 805–809.

10.1021/ja1025744

Ordered mesoporous materials have gained increasing attention because their nanopore channels with large surface area, high porosity, ordered and tunable size can be used as nanoreactors for applications in adsorption, separation and catalysis, and so forth.[24−29] Considerable efforts have recently been devoted to magnetic mesoporous materials to combine the high surface area and magnetic properties; however, most of them focused on the adsorption or drug delivery application, and rare work succeeded in designing magnetic mesoporous materials with multicomponents and well-defined nanostructures for advanced catalysis. Herein, we report, for the first time, a construction of multifunctional magnetic mesoporous microspheres possessing a core of silica-coated magnetite particles, a transition layer of uniform gold nanoparticles and an outer shell of ordered mesoporous silica with perpendicularly aligned pore channels. This unique multicomponent nanostructured material, designated as $Fe_3O_4@SiO_2-Au@mSiO_2$, was fabricated by combining the versatile sol−gel process, interfacial deposition and surfactant-templating synthesis through a multistep approach involving conformal coating of Fe_3O_4 particles with SiO_2, depositing Au nanoparticles, and finally introducing mesoporous silica shell. The designed multifunctional microspheres possess large magnetization, highly open and ordered mesopores, and stably confined but exposed active metal particles. Fast catalytic reduction of 4-nitrophenol (with conversion of 95% in 12 min) in water and efficient epoxidation of styrene with high conversion (72%) and selectivity (80%) were achieved by using the unique multicomponent nanostructured materials as a catalyst. Using an external magnetic field, the catalyst can be easily recycled, and long-life and high reusability are demonstrated without visible decrease in the catalytic performance after running even for more than 10 times.

2. Experimental Section

2.1. Chemicals. Anhydrous $FeCl_3$, trisodium citrate, tetraethyl orthosilicate (TEOS), $HAuCl_4 \cdot 3H_2O$, ethanol, concentrated ammonia solution (28 wt %), styrene, $NaBH_4$, 3-aminopropyl triethylsilane (APTS), *n*-butylamine, $AgNO_3$, and 4-nitrophenol (4-NP) are of analytical grade and purchased from Shanghai Chemical Corp. *t*-Butyl hydroperoxide (70 wt % in water) was supplied by Aldrich-sigma. Styrene was purified by filtrating through Al_2O_3 column. All other chemicals were used as received. Deionized water was used for all experiments.

2.2. Materials for Synthesis of Multicomponent $Fe_3O_4@SiO_2-Au@mSiO_2$ Microspheres. 2.2.1. Synthesis of Fe_3O_4 Particles. The water dispersible Fe_3O_4 particles were synthesized according to the method reported previously.[22] Briefly, $FeCl_3$ (2.6 g, 16 mmol), trisodium citrate (1.0 g, 3.4 mmol), and sodium acetate (NaAc) (4.0 g, 48.8 mmol) were dissolved in ethylene glycol (80 mL) with magnetic stirring. The obtained yellow solution was then transferred and sealed into a Teflon-lined stainless-steel autoclave (200 mL in capacity). The autoclave was heated at 200 °C for 10 h, and then allowed to cool to room temperature. The black products were washed with ethanol and deionized water 3 times, respectively.

2.2.2. Synthesis of $Fe_3O_4@SiO_2$ and APTS-Modified $Fe_3O_4@SiO_2$ Microspheres. The $Fe_3O_4@SiO_2$ microspheres were prepared through a versatile solution sol−gel method as follows. An aqueous dispersion of the magnetite particles (70 mL, 0.02 g/mL) was added to a three-neck round-bottom flask charged with absolute ethanol (280 mL) and concentrated ammonia solution (5.0 mL, 28 wt %) under mechanical stirring for 15 min at 30 °C. Afterward, 4.0 mL of tetraethyl orthosilicate (TEOS) was added dropwise in 2 min, and the reaction was allowed to proceed for 8 h under continuous mechanical stirring. The resultant core−shell $Fe_3O_4@SiO_2$ microsphere product was separated and collected with a magnet, followed by washing with ethanol 6 times. Finally, the product was redispersed in absolute isopropyl alcohol to form a homogeneous dispersion with solid content of ca. 1 wt % for further uses.

For the surface modification, the obtained dispersion (40 mL) containing the $Fe_3O_4@SiO_2$ microspheres was further diluted with isopropyl alcohol (100 mL) containing γ-aminopropyl-triethoxysilane (APTS, 0.2 mL) under ultrasonication in a water bath. The resultant dispersion was bubbled with nitrogen gas for 30 min, and then heated at 70 °C under mild mechanical stirring for 6 h. Finally, with the help of a magnet, the APTS-modified $Fe_3O_4@SiO_2$ microspheres were harvested and repeatedly washed with ethanol and deionized water, and redispersed in water to form a homogeneous dispersion (ca. 0.8 wt %).

2.2.3. Synthesis of Au Nanoparticles. Gold nanoparticles were prepared according to Frens's method.[30] An aqueous solution of $HAuCl_4$ (100 mL, 5.0×10^{-4} M) was prepared and stirred rapidly in a clean and new three-neck round-bottom flask equipped with a condenser. The flask was immerged in an oil bath for heating at 100 °C. When the solution began to be boil, 5.0 mL of prewarmed trisodium citrate solution (1.0 wt %) was added by injection. After further stirring for about 30 min, the violet-red solution containing Au nanoparticles was obtained. The solution was cooled down by magnetically stirring at room temperature for further uses.

2.2.4. Deposition of Au Nanoparticles on APTS-Modified $Fe_3O_4@SiO_2$ Microspheres. In an optimized deposition process, 30 mL of the Au nanoparticle solution was mixed with 50 mL of aqueous dispersion of APTS-$Fe_3O_4@SiO_2$ microspheres by quick ultrasonication in a water bath. The mixture was subjected to mechanical stirring for 3 h, and the $Fe_3O_4@SiO_2-Au$ microspheres were separated, wand washed with deionized water 6 times.

2.2.5. Synthesis of $Fe_3O_4@SiO_2-Au@mSiO_2$ Microspheres. To grow a mesoporous silica shell on the $Fe_3O_4@SiO_2-Au$ microspheres, the as-made $Fe_3O_4@SiO_2-Au$ microspheres (0.12 mg) were employed as seeds and redispersed in a mixed solution containing CTAB (0.45 g, 1.2 mmol), deionized water (100 mL), concentrated ammonia solution (2.0 mL, 28 wt %), and ethanol (150 mL). The resultant mixed solution was ultrasonicated for 5 min and then mechanically stirred for 30 min to form a uniform dispersion. Subsequently, 1.5 mL of TEOS was added dropwise to the dispersion under continuous stirring. After stirring for 6 h at 30 °C, the product was collected with a magnet and washed repeatedly with ethanol and deionized water. Finally, the purified microspheres were redispersed in 100 mL of acetone and refluxed at 80 °C for 48 h to remove the template CTAB. The extraction was repeated 6 times to ensure a complete removal of CTAB templates. Finally, the products were washed with deionized water, and $Fe_3O_4@SiO_2-Au@mSiO_2$ microspheres with 90 nm-thick mesoporous silica were obtained. The successful removal of CTAB was verified by FT-IR analysis. To obtain microspheres with mesoporous silica thickness of 40 and 20 nm, 0.18 and 0.20 mg of

(22) Liu, J.; Sun, Z. K.; Deng, Y. H.; Zou, Y.; Li, C. Y.; Guo, X. H.; Xiong, L. Q.; Gao, Y.; Li, F. Y.; Zhao, D. Y. *Angew. Chem., Int. Ed.* **2009**, *48*, 5875–5879.
(23) Deng, Y. H.; Deng, C. H.; Qi, D. W.; Liu, C.; Liu, J.; Zhang, X. M.; Zhao, D. Y. *Adv. Mater.* **2009**, *21*, 1377–1382.
(24) Kresge, C. T.; Leonowicz, M. E.; Roth, W. J.; Vartuli, J. C.; Beck, J. S. *Nature* **1992**, *359*, 710–712.
(25) Zhao, D. Y.; Feng, J. L.; Huo, Q. S.; Melosh, N.; Fredrickson, G. H.; Chmelka, B. F.; Stucky, G. D. *Science* **1998**, *279*, 548–552.
(26) Corma, A. *Chem. Rev.* **1997**, *97*, 2373–2419.
(27) Deng, Y. H.; Yu, T.; Wan, Y.; Shi, Y. F.; Meng, Y.; Gu, D.; Zhang, L. J.; Huang, Y.; Liu, C.; Wu, X. J.; Zhao, D. Y. *J. Am. Chem. Soc.* **2007**, *129*, 1690–1697.
(28) Joo, S. H.; Park, J. Y.; Tsung, C. K.; Yamada, Y.; Yang, P. D.; Somorjai, G. A. *Nat. Mater.* **2009**, *8*, 126–131.
(29) Zhu, Y. F.; Kockrick, E.; Ikoma, T.; Hanagata, N.; Kaskel, S. *Chem. Mater.* **2009**, *21*, 2547–2553.
(30) Frens, G. *Nature (London), Phys. Sci.* **1973**, *241*, 20–22.

the Fe_3O_4@SiO_2−Au microspheres were used for the CTAB-involved sol−gel process while keeping other reaction conditions unchanged.

2.3. Catalytic Reduction of 4-Nitrophenol (4-NP). The reduction of 4-NP was carried out in a quartz cuvette and monitored using a UV−vis spectroscopy (Jasco V-550) at room temperature (25 °C). For comparison, the yellow aqueous 4-NP solution (0.01 M) was prepared and measured prior to monitoring the changes of absorption. A total of 0.10 mL of aqueous 4-NP solution (0.005 M) was mixed with 1.0 mL of fresh $NaBH_4$ (0.2 M) solution. Subsequently, 1.0 mL of aqueous dispersion of the Fe_3O_4@SiO_2−Au@mSiO_2 microspheres (0.3 wt %) was added, and solution was quickly subjected to UV−vis measurements; therefore, the obtained data can be designated as the value for reaction time $t = 0$. Afterward, the solution was *in situ* measured every 3 min to obtain the successive information about the reaction. In fact, as the reaction proceeds, one could observe the gradual change of the solution color from yellow to colorless.

To study the reusability of the magnetic catalysts, the used magnetic microspheres were separated from the solution with a magnet after the monitoring whole reduction process was completed. The recycled magnetic microspheres were washed with ethanol 6 times and with deionized water 3 times. Similar to the above reduction process, the obtained magnetic microspheres were redispersed with 1.0 mL of deionized water and mixed with 0.1 mL of aqueous 4-NP solution (0.005 M) and 1.0 mL of fresh $NaBH_4$ (0.2 M) solution. After reaction for 20 min, the solution was measured using UV−vis spectroscopy. The procedure was repeated more than 10 times. No significant decrease in the 4-NP conversion was detected.

2.4. Styrene Catalyzed Epoxidation. Styrene epoxidation reaction over the magnetic composite catalysts was carried out at atmospheric pressure. A mixture of the magnetic composite catalyst (0.10 g), styrene (1.3 mL, 10 mmol), and acetonitrile (15 mL) was first magnetically stirred for 30 min under a high purity nitrogen atmosphere at room temperature. After adding 5.0 g (38 mmol) of *t*-butyl hydroperoxide (70 wt % in water), the reaction vessel was immersed in an oil bath and heated at 82 °C. During the reaction process, a minor amount of reaction solution (∼30 μL) was carefully withdrawn after a certain time for gas chromatography measurements. Before each sampling, the stirring was temporarily stopped to cause the aggregation of the microspheres on the magnetic stir bar and to avoid loss of the catalyst during sampling. After reaction for 40 h, the reaction system was cooled down, and the catalyst was recycled using a magnet and washed with acetonitrile 6 times and with deionized water another 6 times. The reaction was repeated with the recycled magnetic catalyst for more than 10 times and each reaction was conducted for 20 h.

2.5. Measurements and Characterizations. Transmission electron microscopy (TEM) images were taken with a JEOL 2011 microscope (Japan) operated at 200 kV. Samples were first dispersed in ethanol and then collected using carbon-film-covered copper grids for analysis. Scanning electronic microscopy (SEM) images were recorded on a Philips XL30 electron microscope (The Netherlands) operating at 20 kV. A thin gold film was sprayed on the sample before measurements. Fourier-transform infrared (FT-IR) spectra were collected on Nicolet Fourier spectrophotometer using KBr pellets. Powder X-ray diffraction (XRD) patterns were recorded on a Bruker D4 X-ray diffractometer (Germany) with Ni-filtered Cu Kα radiation (40 kV, 40 mA). Nitrogen sorption isotherms were measured at 77 K with a Micromeritcs Tristar 3000 analyzer. Before measurements, the samples were degassed in a vacuum at 200 °C for 10 h. The Brunauer−Emmett−Teller (BET) method was utilized to calculate the specific surface areas (S_{BET}) using adsorption data in a relative pressure range from 0.005 to 0.25. By using the Barrett−Joyner−Halenda (BJH) model, the pore volumes and pore size distributions were derived from the adsorption branches of isotherms, and the total pore volumes (V_t) were estimated from the adsorbed amount at a relative pressure P/P_0 of 0.992. The metal contents in the Fe_3O_4@SiO_2−Au@mSiO_2 samples were measured using inductively coupled plasma-atomic emission spectrometry (ICP-AES, Varian VISTA-MPX). The UV−vis spectra were recorded on a UV−vis spectrometer (Jasco V-550) at 25 °C. The epoxidation reaction products and unconverted reactants were analyzed by gas chromatography−mass spectrometry using HP-5MS capillary column and He as carrier gas.

3. Results and Discussion

3.1. Synthesis of Fe_3O_4@SiO_2−Au@mSiO_2 Microspheres. The magnetite particles were prepared via a robust solvothermal reaction based on a high temperature reduction of Fe(III) salts with ethylene glycol in the presence of trisodium citrate.[22] As revealed by transmission electron microscopy (TEM), the obtained magnetite particles are uniform with a mean diameter of ∼200 nm (Figure 1a). Selected area electron diffraction (SAED) pattern patterns exhibit spotty diffraction rings, indicating a polycrystalline feature (Figure 1a, inset). High-resolution TEM (HRTEM) images clearly show that each magnetite particle is composed of plentiful nanocrystals with the size of about 8.0 nm (Figure 1b). Scanning electron microscopy (SEM) image of the magnetite particles further confirms the uniform size of ∼200 nm and nearly spherical shape with rough surface (Figure 2a). The surface roughness is attributed to the fact that the particles are formed by packing many nanocrystals. The magnetite particles are capped with citrate groups and exhibit excellent dispersibility in polar solvents such as water and ethanol, which favors the subsequent coating or modification with other oxides or polymers. Through a sol−gel process by the hydrolysis and condensation of tetraethyl orthosilicate (TEOS) in ethanol/ammonia mixture, uniform silica layer (∼30 nm in thickness) can be formed on individual magnetite particle seed, resulting in core−shell Fe_3O_4@SiO_2 microspheres (Figure 1c). Compared with the magnetite particles, the obtained Fe_3O_4@SiO_2 microspheres (Figure 2b) exhibit more regular spherical shape with smooth surface due to the deposition and growth of silica occurring on a molecular scale in the sol−gel process.[31,32]

To deposit Au nanoparticles efficiently, Fe_3O_4@SiO_2 microspheres were modified with 3-aminopropyl triethylsilane (APTS) to endow abundant amino groups on surface, which can enhance the interaction with gold by coordination bonds.[16] Fourier transform infrared (FT-IR) spectra confirmed the successful surface modification, and the Fe_3O_4@SiO_2−NH_2 microspheres were obtained (Figure S1). Gold nanoparticles were prepared by citrate reduction of $HAuCl_4$ in aqueous solution according to Frens's method.[30] TEM images show that the obtained gold nanoparticles have uniform size of about 12 nm (Figure 1d). After incubation with Fe_3O_4@SiO_2−NH_2 microspheres in solution, the gold nanoparticles can deposit on the surface of microspheres. TEM images of the resulting Fe_3O_4@SiO_2−Au microspheres clearly show that the surface is evenly covered by Au nanoparticles (Figure 1e, Figure S2), which is mainly driven by the ligand exchange of citrates to the amino groups.[11] Notably, we can vary the grafting density of APTS molecules to control the number of Au nanoparticles deposited on the Fe_3O_4@SiO_2 microspheres (Figure 1f). UV−vis absorption spectra (Figure 3a) show a plasmon resonance band at 520 nm, characteristic of the Au nanoparticles with the size of 12−15

(31) Stöber, W.; Fink, A.; Bohn, E. *J. Colloid Interface Sci.* **1968**, *26*, 62–69.
(32) Van, B. A.; Van, G. J.; Vrij, A. *J. Colloid Interface Sci.* **1992**, *154*, 481–501.

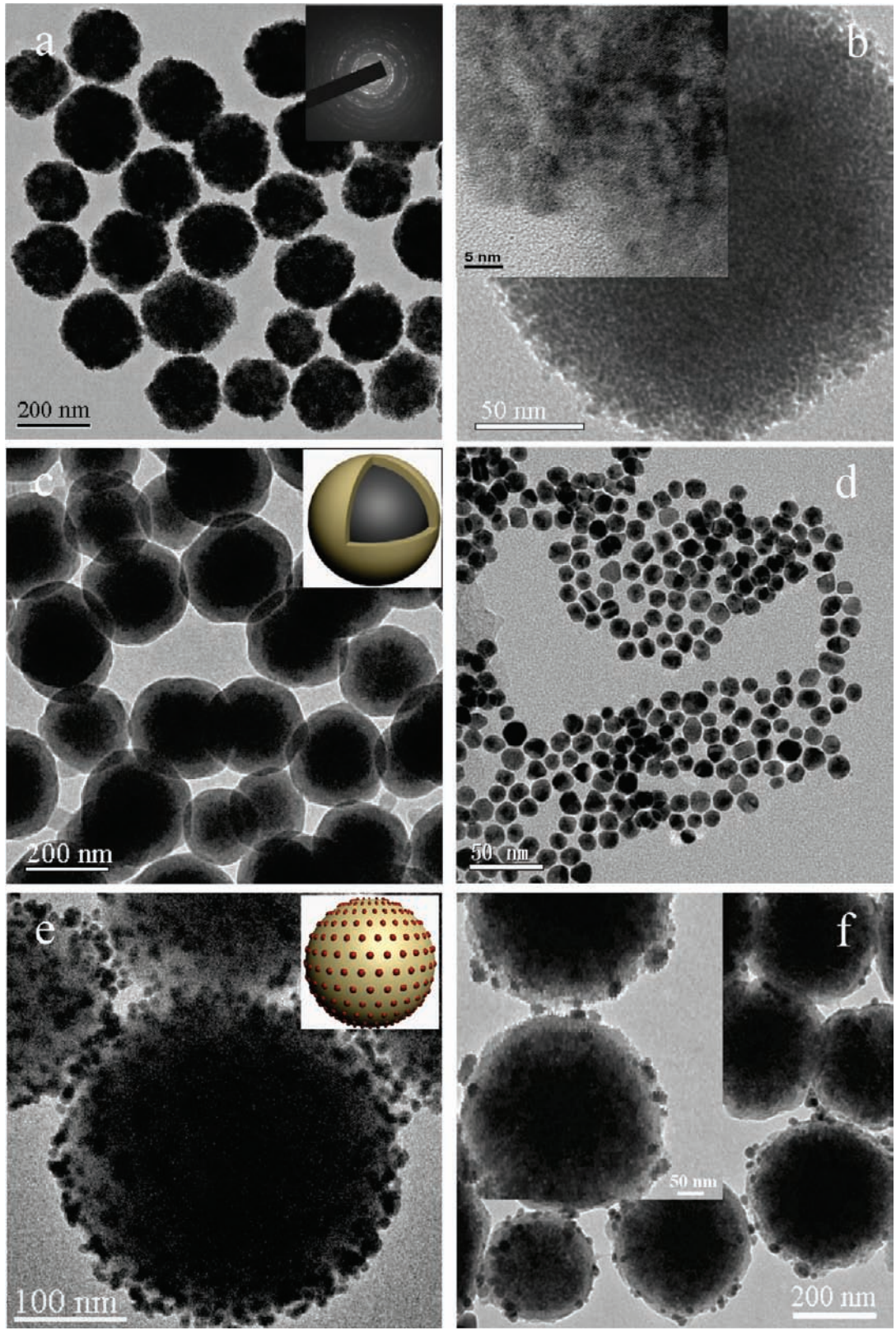

Figure 1. TEM images of (a and b) Fe_3O_4 particles, (c) $Fe_3O_4@SiO_2$ microspheres, (d) Au nanoparticles, (e and f) $Fe_3O_4@SiO_2-Au$ microspheres with different loading amount of Au nanoparticles. Inset (a) is the SAED pattern recorded on single particle; insets (c and e) are the structural models for the $Fe_3O_4@SiO_2$ and $Fe_3O_4@SiO_2-Au$ microspheres, respectively. Insets (b and f) are enlarged TEM images.

nm in aqueous solution.[33] In contrast, the $Fe_3O_4@SiO_2-Au$ microsphere dispersion exhibits a broad absorption band at 589 nm (Figure 3a), indicating a red shift of about 89 nm, due to the deposition of Au nanoparticles on the surface.[34] Our results show that without prior surface modification with amino groups, almost no Au nanoparticles deposit on the microspheres due to insufficient interaction. Wide-angle XRD patterns of the $Fe_3O_4@SiO_2-Au$ microspheres show the characteristic broad

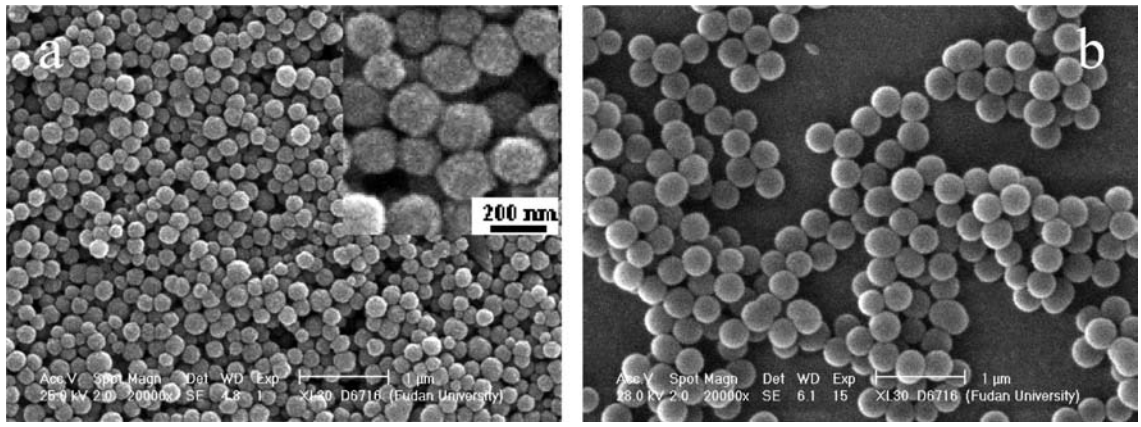

Figure 2. SEM images of the magnetite particles before (a) and after (b) the silica coating. Inset (a) is high-magnification SEM image.

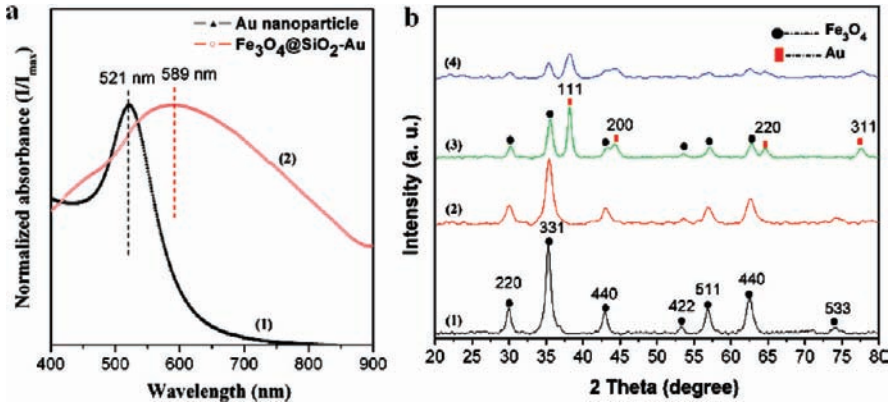

Figure 3. (a) UV−vis spectra of (1) Au nanoparticles aqueous dispersion (dark triangles) and (2) $Fe_3O_4@SiO_2-NH_2-Au$ microspheres aqueous dispersion (red cycles). (b) The wide-angle XRD patterns of (1) Fe_3O_4 particles, (2) $Fe_3O_4@SiO_2$ microspheres, (3) $Fe_3O_4@SiO_2-Au$ microspheres, and (4) $Fe_3O_4@SiO_2-Au@mSiO_2$ microspheres.

diffraction peaks indexed to the cubic-phase Au and spinel Fe_3O_4 nanoparticles, further proving the attachment of Au nanoparticles and the well-retained magnetite phase (Figure 3b). According to the Debye−Scherrer formula, the nanocrystal size is calculated to be 12.2 and 8.3 nm for Au and magnetite nanoparticles, respectively, well agreeing with that from TEM observations.

As the Au nanoparticles are negatively charged with citrate groups, the $Fe_3O_4@SiO_2-Au$ microspheres can be well dispersed in water, favoring the further surface coating. Through a surfactant-assembly sol−gel process with TEOS as a silica source and cetyltrimethylammonium bromide (CTAB) as a structure-directing agent, a mesostructred CTAB/silica composite layer can be formed on the $Fe_3O_4@SiO_2-Au$ microspheres. After the removal of CTAB template by acetone extraction, mesoporous silica shell can be obtained. TEM images show that the $Fe_3O_4@SiO_2-Au$ microspheres are uniformly coated by a layer of mesoporous silica with thickness of ∼90 nm (Figure 4a), resulting in well-defined sandwich structure of $Fe_3O_4@SiO_2-Au@mSiO_2$ microspheres. Furthermore, the mesopore channels are found to be perpendicular to the surface as shown in HRTEM images (Figure 4b). The unique pore orientation is attributed to the preferred alignment of surfactant/siliceous oligomer composites to the preformed colloidal particles, which may help to significantly decrease the interface energy in the system. The previous literature based on electron microscopy techniques, electron crystallography, and Monte Carlo simulations reveals that such a preferred alignment is due to the interface between the silica/surfactant phase and the ethanol/water solution being equally attractive toward polar and nonpolar species, which can induce perpendicular alignment of surfactant mesophases.[35−37]

Low-angle XRD patterns (Figure 4c) of the $Fe_3O_4@SiO_2-Au@mSiO_2$ microspheres display three resolved diffraction peaks assigned to the 100, 110, 200 reflections of a 2-D hexagonal mesostructure (Figure 3, inset). N_2 sorption−desorption isotherms of the microspheres show representative type-IV curves, suggesting cylindrical pores with a narrow pore size distribution at 2.2 nm (Figure 4d). The BET surface area and total pore volume are calculated to be as high as 236 m^2/g and 0.21 cm^3/g, respectively. The magnetization saturation values were measured to be 64.1, 39.6, 37.0, and 18.6 emu/g for Fe_3O_4, $Fe_3O_4@SiO_2$, $Fe_3O_4@SiO_2-Au$, and $Fe_3O_4@SiO_2-Au@mSiO_2$, respectively (Figure S5). It reveals a weight content of ∼29% and ∼2.0% for magnetite particles and Au nanoparticles in the $Fe_3O_4@SiO_2-Au@mSiO_2$ microspheres, respectively, which is consistent to the results (20 wt % for Fe and 2.2 wt % for Au) determined from the elemental analysis of inductively coupled plasma-atomic emission spectrometry (ICP-AES). All the

(33) Link, S.; El-Sayed, M. A. *J. Phys. Chem. B* **1999**, *103*, 4212–4217.
(34) Storhoff, J. J.; Lazarides, A. A.; Mucic, R. C.; Mirkin, C. A.; Letsinger, R. L.; Schatz, G. C. *J. Am. Chem. Soc.* **2000**, *122*, 4640–4650.
(35) Tan, B.; Rankin, S. E. *J. Phys. Chem. B* **2004**, *108*, 20122–20129.
(36) Yoon, S. B.; Kim, J. Y.; Kim, J. H.; Park, Y. J.; Yoon, K. R.; Park, S. K.; Yu, J. S. *J. Mater. Chem.* **2007**, *17*, 1758–761.
(37) Rankin, S. E.; Malanoski, A. P.; van Swol, F. *Mater. Res. Soc. Symp. Proc.* **2001**, *636*, 121.

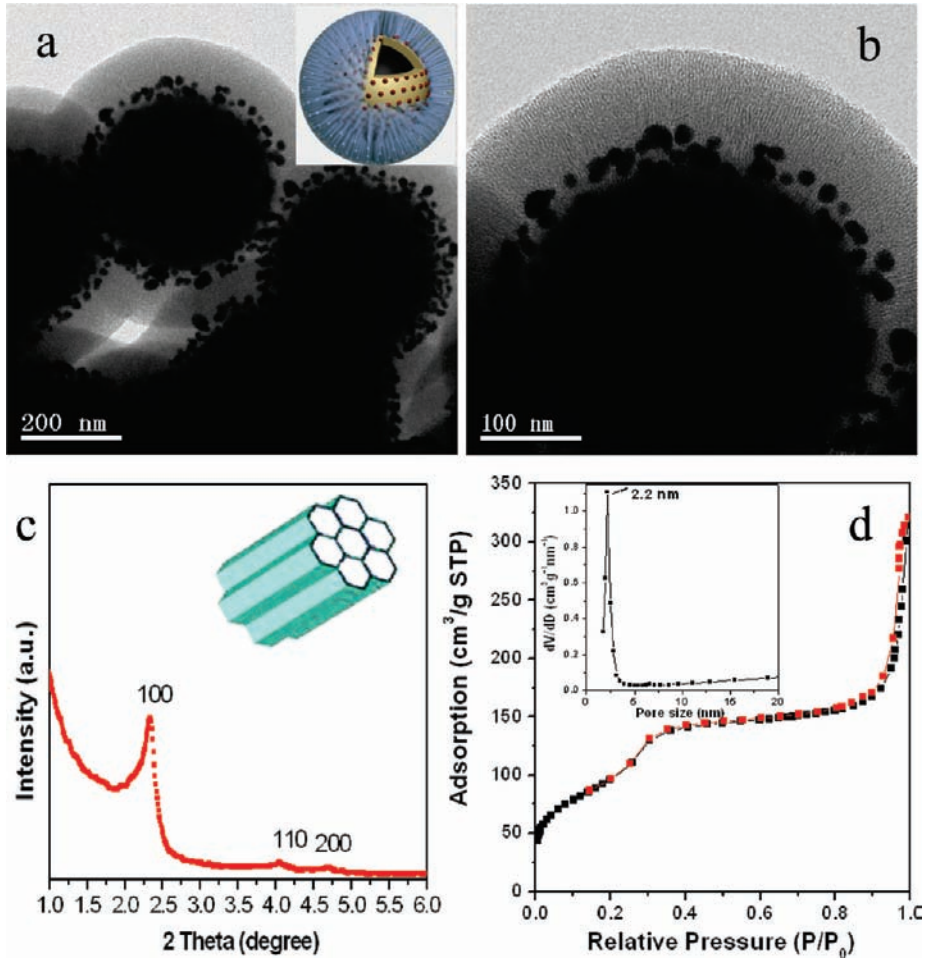

Figure 4. (a and b) TEM images of the $Fe_3O_4@SiO_2-Au@mSiO_2$ microspheres with an 90-nm thick mesoporous silica layer, (c) the low-angle XRD pattern of the $Fe_3O_4@SiO_2-Au@mSiO_2$ microspheres, (d) the nitrogen adsorption−desorption isotherms and pore size distribution (inset) of the $Fe_3O_4@SiO_2-Au@mSiO_2$ microspheres with an 90-nm thick mesoporous silica layer. Inset (a) is a structural model of the $Fe_3O_4@SiO_2-Au@mSiO_2$ microspheres; Inset (c) is a structural model of the mesoporous silica shells, showing 2-D hexagonal cylinder symmetry.

magnetic samples show a superparamagnetic behavior as shown in the hysteresis loops (Figure S3). No remanence or coercivity was detected at room temperature due to the fact that the particles are composed of ultrafine magnetite nanocrystals. The superparamagentic property helps to prevent the Au-loaded magnetic microspheres from aggregation, which is important for maximization of the exposure of catalysts for efficient liquid-phase catalysis. As a result of the high magnetite content, the $Fe_3O_4@SiO_2-Au@mSiO_2$ microsphere can be readily separated from its dispersion in less than 1 min by simply using a magnet. The well-defined architecture and highly integrated functionalities of the multicomponent $Fe_3O_4@SiO_2-Au@mSiO_2$ microspheres make them an ideal candidate for diverse applications, particularly in catalysis. The nonporous silica layer on the magnetite particles helps to prevent them from etching in some harsh media. The unique highly open mesopore channels in the outer layer favor the access of guest molecules, serving as nanoreactors. Importantly, since the catalytic Au nanoparticles are effectively immobilized between the nonporous and porous silica layers, they are easily accessible, highly stable and anti-aggregation, and thus reusable with extra-long life in practical applications. To investigate thermal stability, the $Fe_3O_4@SiO_2-Au@mSiO_2$ microspheres and a 3-D ordered macroporous silica monolith loaded with the same Au nanoparticles (pore size of ∼300 nm, window size of ∼50 nm, see Supporting Information for experimental details) were both annealed at 300 °C in argon. The TEM and wide-angle XRD measurements indicate that the mesostructure of the porous silica layer and Au nanoparticles are well-retained in the $Fe_3O_4@SiO_2-Au@mSiO_2$ microspheres and no dramatic agglomeration of Au particles is observed, while the Au nanoparticles in the 3-D ordered macroporous silica are found to grow into irregular larger particles of 30−65 nm. These results clearly indicate that the obtained multicomponent composite microspheres with tightly trapped Au nanoparticles possess higher thermal stability, which is due to the confinement effect exerted by the mesoporous silica shells.

The synthesis of the multifunctional microspheres is well controllable. By simply changing the amount of the $Fe_3O_4@SiO_2-Au$ microspheres, the thickness of mesoporous silica shells can be tuned in the range of 20−100 nm, meanwhile keeping the pore orientation perpendicular to the surface (Figure S4). Moreover, by using this simple approach, other metal nanoparticles or quantum dots can also be sandwiched in the nanostructures. For example, Ag nanoparticles can be directly deposited on microspheres by the *in situ* reduction and form $Fe_3O_4@SiO_2-Ag$ microspheres (Figure S5a). Subsequently, through the CTAB-assembly sol−gel coating process, a layer of uniform mesoporous silica can be produced, resulting in $Fe_3O_4@SiO_2-Ag@mSiO_2$ microspheres with well-defined architecture and 2-D hexagonal symmetry (Figure S5b).

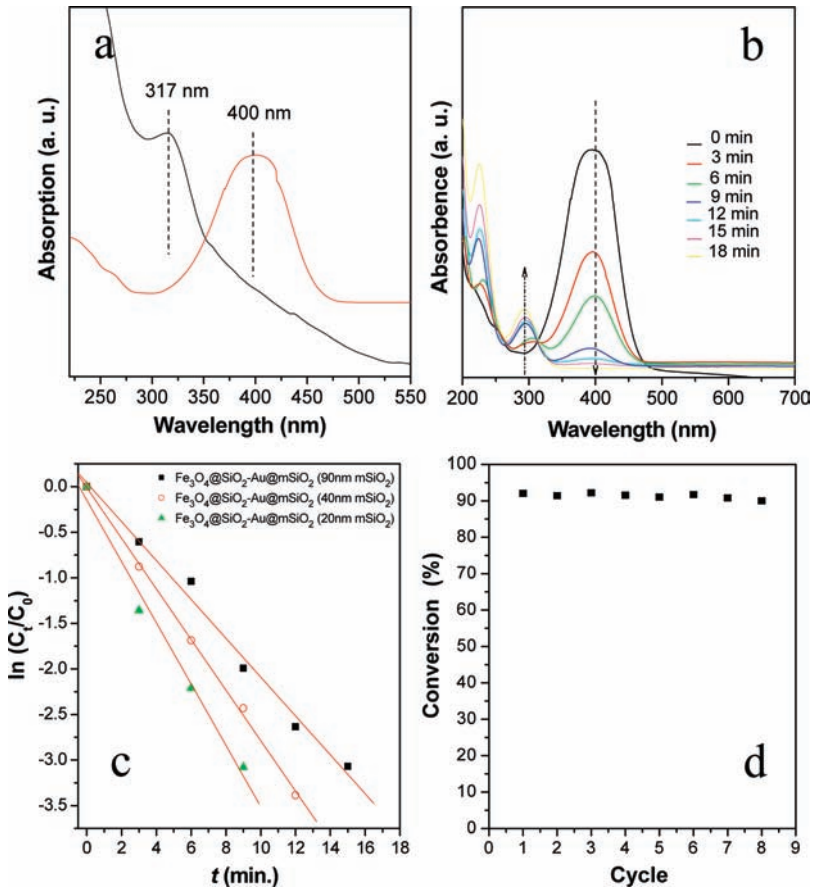

Figure 5. (a and b) UV−vis spectra of (a) 4-nitrophenol before and after adding $NaBH_4$ solution, (b) the reduction of 4-nitrophenol in aqueous solution recorded every 3 min using the $Fe_3O_4@SiO_2-Au@mSiO_2$ microspheres (90-nm thick mesoporous silica shell) as a catalyst, (c) the relationship between $\ln(C_t/C_0)$ and reaction time (t), wherein, the ratios of 4-NP concentrations (C_t at time t) to its initial value C_0 ($t = 0$) were directly given by the relative intensity of the respective absorbance A_t/A_0, and therefore, the reduction course could be directly reflected by these absorption curves. (d) The reusability of the $Fe_3O_4@SiO_2-Au@mSiO_2$ microspheres (90-nm thickness of mesoporous silica shells) as a catalyst for the reduction of 4-nitrophenol with $NaBH_4$.

3.2. Application of $Fe_3O_4@SiO_2-Au@mSiO_2$ Microspheres for Catalytic Reduction of 4-NP. The reduction of 4-NP by sodium borohydride was chosen as a model reaction[38−40] for studying the catalytic performances of multifunctional $Fe_3O_4@SiO_2-Au@mSiO_2$ microspheres. The light yellow aqueous 4-NP solution shows absorption at ∼317 nm. After addition of sodium borohydride, the absorption maximum shifts to 400 nm (Figure 5a) due to the formation of 4-nitorphenolate.[38] No change in the absorption was determined even after standing for 10 h, indicating that the reduction does not proceed without catalyst. After addition of a small amount (3.0 mg) of the $Fe_3O_4@SiO_2-Au@mSiO_2$ microspheres, the absorption peak at 400 nm significantly decreases as the reaction proceeds; meanwhile, a new peak appears at 295 nm and gradually increases, revealing the reduction of 4-NP to form 4-AP (Figure 5b).[38] The UV−vis spectra show an isosbestic point (313 nm), suggesting that the catalytic reduction of 4-NP gives 4-AP only without byproduct. Considering the reductant concentration is much higher than that of 4-NP ($C_{NaBH4}/C_{4\text{-}NP} = 400$), the reaction should be of first order with regard to the reactant. Linear relationships between $\ln(C_t/C_0)$ and reaction time are obtained in the reduction catalyzed by different $Fe_3O_4@SiO_2-Au@mSiO_2$ microspheres (Figure 5c), which well match the first-order reaction kinetics. The rate constant k was calculated to be 0.20, 0.28, and 0.35 min^{-1} for the reactions using magnetic catalysts with mesoporous silica thickness of 90, 40, and 20 nm, respectively. These results indicate that decreasing the mesoporous shell thickness can help to increase the catalysis efficiency, which is mainly due to the shorter diffusion distance and thus better mass diffusion for the catalysis with thinner mesoporous shell. For comparison, the reduction reactions using unprotected $Fe_3O_4@SiO_2-Au$ microspheres were also carried out under the same conditions. It is found that, in the first run, the catalyst shows very fast catalysis with a rate constant of 0.42, which is due to the complete exposure of Au nanoparticle in the solution. However, the rate constant decreases significantly to 0.26, 0.18, and 0.07 in the second, third, and fourth runs, respectively, suggesting a poor stability and reusability, which is due to the detachment of Au nanoparticles from the microspheres surface during cycles.

To investigate the reusability, the $Fe_3O_4@SiO_2-Au@mSiO_2$ microspheres were separated using a magnet from the catalytic reaction solution. The catalyst exhibits similar catalytic performance without visible reduction in the conversion for the same reaction time (20 min) even after running for more than 7 cycles (Figure 5d). Our TEM measurements show that the microstructures of the multifunctional microspheres including the inside Au nanoparticles are well retained after plenty of repeating catalytic processes, further suggesting an excellent stability and long life.

(38) Pradhan, N.; Pal, A.; Pal, T. *Langmuir* **2001**, *17*, 1800–1802.
(39) Pradhan, N.; Pal, A.; Pal, T. *Colloids Surf. A* **2002**, *196*, 247–257.
(40) Ghosh, S. K.; Mandal, M.; Kundu, S.; Nath, S.; Pal, T. *Appl. Catal., A* **2004**, *268*, 61–66.

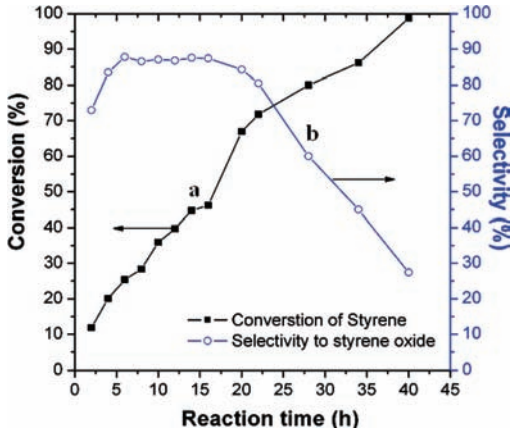

Figure 6. Epoxidation of styrene by using anhydrous *t*-butyl hydroperoxide (TBHP) as an oxidant over the $Fe_3O_4@SiO_2-Au@mSiO_2$ microspheres with 90-nm thickness of mesoporous silica shells at 82 °C. The conversion of styrene and selectivity of styrene oxide were functioned with the reaction time.

3.3. Application of $Fe_3O_4@SiO_2-Au@mSiO_2$ Microspheres for Catalytic Epoxidation of Styrene. Our results show that this novel multifunctional microsphere can be used as a highly active catalyst not only in room temperature reaction, but also in higher temperature process at around 80 °C. The catalytic epoxidation of styrene with *t*-butyl hydroperoxide (TBHP) as an oxidant at 82 °C was investigated using the multifunctional microspheres as catalysts. It is known that Au-nanoparticle catalysts[41−44] show high conversion and good selectivity; however, it suffers possibility of being washed away and disengaged from the supports during recycling. Our well-designed supported catalyst $Fe_3O_4@SiO_2-Au@mSiO_2$ microspheres hold great promise to overcome these problems. The conversion of styrene increases continuously as the reaction time and can reach as high as 98% for 40 h (Figure 6a). The selectivity to styrene oxide dramatically increases from 73 to 88% and is maintained at ∼87% in the following 10 h. Further prolonging the time leads to a decrease in selectivity (Figure 6b), which is mainly caused by the isomerization of styrene oxide or overoxidation at high temperature reaction. Taking a comprehensive consideration of the conversion and selectivity, it is concluded that our magnetic catalyst can achieve high conversion (72%) and selectivity (80%) after reaction for 20 h, which is comparable or/and higher than previous work.[45,46] In addition, the magnetic catalyst can be easily separated from the reaction system with a magnet, and no significant decrease in both conversion and selectivity is observed after running for more than 10 times. Wide-angle XRD and electronic microscope measurements indicate that the composition (crystalline phases) and microstructures of the multifunctional microspheres are well retained after >10 recycles. The high catalytic performance of the microspheres should be attributed to their large surface area and highly open mesochannels, the excellent accessibility, good dispersion and high stability of the confined Au nanoparticles.

4. Conclusion

In summary, we demonstrate a successful synthesis of multicomponent and multifunctional $Fe_3O_4@SiO_2-Au@mSiO_2$ microspheres with well-defined core−shell nanostructures, confined catalytic gold nanoparticles and accessible ordered mesopore channels by combining the sol−gel process, interfacial deposition, and surfactant-templating approach. The well-designed microspheres have high magnetization (18.6 emu/g), highly open and ordered mesopores (∼2.2 nm in diameter), stably confined but exposed catalytic metal nanoparticles that uniformly dispersed between the Fe_3O_4 core, and ordered mesoporous silica shell. The obtained multifunctional microspheres show excellent catalytic performance in room temperature reduction of 4-nitrophenol (high activity of 95%) and highly selective epoxidation of styrene (selectivity >80%) at 82 °C both with convenient separability and excellent reusability without visible loss in mass and activity. Therefore, this functional nanostructure holds great promise as a novel gold-based catalyst system for various catalytic reactions. Additionally, the design concept for the multifunctional nanomaterials can be extended to the fabrication of other mulitcomponent nanosystems with integrated and enhanced properties for various advanced applications, such as chemical/biosensor, nanoelectronics, and so on.

Acknowledgment. This work was supported by NSF of China (20890120, 20721063, 20821140537, 20871030), State Key Basic Research Program of PRC (2006CB932302, 2006CB202502 and 2009AA033701), Shanghai Leading Academic Discipline Project (B108), Shanghai Rising Star Program for Young Research Scientists (08QA14010), Doctoral Program Foundation of State Education Commission of China (200802461013), and Science & Technology Commission of Shanghai Municipality (08DZ2270500).

Supporting Information Available: Experimental details for thermal stability studies and synthesis of $Fe_3O_4@SiO_2-Ag@mSiO_2$ microspheres, FT-IR spectra of the $Fe_3O_4@SiO_2$ microspheres before and after surface modification with 3-aminopropyltriethylsilane (APTS), TEM images of the $Fe_3O_4@SiO_2-Au$ microspheres with a lower magnification, the magnetic hysteresis loops of Fe_3O_4 particles, $Fe_3O_4@SiO_2$ microspheres, the $Fe_3O_4@SiO_2-Au$ microspheres and $Fe_3O_4@SiO_2-Au@mSiO_2$ microspheres with 90-nm thickness outer mesoporous silica layer, TEM images of the $Fe_3O_4@SiO_2-Au@mSiO_2$ microspheres with 40-nm and 20-nm thick mesoporous silica shells, and TEM images of $Fe_3O_4@SiO_2-Ag$ particles and $Fe_3O_4@SiO_2-Ag@mSiO_2$ microspheres. This material is available free of charge via the Internet at http://pubs.acs.org.

JA1025744

(41) Haruta, M.; Kobayashi, T.; Sano, H.; Yamada, N. *Chem. Lett.* **1987**, 405–406.
(42) Daniel, M. C.; Astruc, D. *Chem. Rev.* **2004**, *104*, 293–346.
(43) Patil, N. S.; Uphade, B. S.; Jana, P.; Bharagav, S. K.; Choudhary, V. R. *J. Catal.* **2004**, *223*, 236–239.
(44) Jin, Y.; Wang, P. J.; Yin, D. H.; Liu, J. F.; Qiu, H. Y.; Yu, N. Y. *Microporous Mesoporous Mater.* **2008**, *111*, 569–576.
(45) Kumar, S. B.; Mirajkar, S. P.; Pais, G. C. G.; Kumar, P.; Kumar, R. *J. Catal.* **1995**, *156*, 163–166.
(46) Xu, R.; Wang, D. S.; Zhang, J. Y.; Li, Y. D. *Chem.−Asian J.* **2006**, *1*, 888–893.